ATLAS NOTE

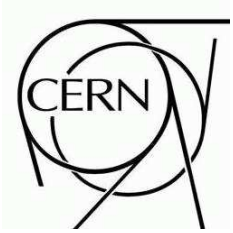

January 23, 2009

Calibration of ATLAS Tile Calorimeter at Electromagnetic Scale

K.J. Anderson[1], L. Bať ková[2], M. Cavalli-Sforza[3], T. Carli[4], M. Cascella[5], T. Davídek[6], T. Del Prete[5], T. Djobava[7], A. Dotti[5], R. Febbraro[8], N. Gollub[4], H. Hakobyan[9], A. Henriques[4], M.H. Hurwitz[10], A. Isaev[11], I. Jen-La Plante[10], A. Karyukhin[11], H. Khandanyan[12], J. Khramov[13], Y. Kulchitsky[14][13], M. Makouski[11], M. Mosidze[7], A. Myagkov[11], J.E. Pilcher[10], L. Přibyl[4][15], M. Rullgard[16], C. Santoni[8], N. Shalanda[11], A. Solodkov[11], O. Solovyanov[11], J. Starchenko[11], P. Šťavina[2], M. Simonyan[17][9], R.J. Teuscher[10], P. Tsiareshka[13][14], E. Vichou[12], V. Vinogradov[13], I. Vivarelli[18], M. Volpi[3], T. Ženiš[2]

[1] University of Chicago, USA
[2] Comenius University, Bratislava, Slovakia
[3] Inst. de Fisica de Altas Energias (IFAE) Universidad Autonoma de Barcelona, Spain
[4] CERN, Geneva, Switzerland
[5] INFN, Sezione di Pisa, Italy
[6] Charles University in Prague, Faculty of Mathematics and Physics, Prague, Czech Republic
[7] HEPI, Tbilisi State University, Tbilisi, Georgia
[8] LPC Clermont–Ferrand, Université Blaise Pascal, Clermont-Ferrand, France
[9] Yerevan Physics Institute, Armenia
[10] Enrico Fermi Institute, University of Chicago, USA
[11] Institute for High Energy Physics, Protvino, Russia
[12] University of Illinois, Urbana-Champaign, Illinois, USA
[13] JINR, Dubna, Russia
[14] Institute of Physics, National Academy of Sciences, Minsk, Belarus
[15] Institute of Physics, Academy of Sciences of the Czech Republic, Prague, Czech Republic
[16] Department of Physics Stockholm University, Sweden
[17] lapp-Laboratoire d'Annecy-le-Vieux de Physique des Particules, Inst. Nat. Phys. Nucl. et Particul. (IN2P3), France.
[18] Pisa University and INFN, Pisa, Italy

ATL-TILECAL-PUB-2009-001
06 February 2009

Abstract

Test beam studies were performed with 11% of the production ATLAS Tile Calorimeter modules. In this paper we summarize the measurement of the electromagnetic (EM) scale calibration constant for over 200 calorimeter cells exposed to electron and muon test beams at CERN SPS accelerator. The Tile Calorimeter modules are currently installed in the ATLAS detector. The analysis presented in this paper takes into account the recent improvements in the Tile Calorimeter cesium calibration, charge injection system calibration and Fit Method energy reconstruction. The overall conversion factor between the measured charge and the energy deposited by measured particles for over 200 Tile Calorimeter cells is 1.050 ± 0.003 pC/GeV, with spread of $2.4 \pm 0.1\%$. We discuss in detail the sources of uncertainties of EM scale calibration constant.

We also show, that after inter-calibrating all the Tile Calorimeter cells with a radioactive cesium source and setting the EM scale in the first calorimeter compartment with electron beams, the values of signals measured in the second and third calorimeter compartment need to be increased by 1–9% to keep the EM scale uniform in the whole calorimeter.

1 Introduction

The ATLAS detector [1] at the proton-proton Large Hadron Collider (LHC) is ready to measure the first particle collisions and the calorimeter system will play an essential role in the measurement of jet energies and missing energy. The key role of the ATLAS detector calorimeters is the absolute measurement of energy deposited by particles crossing the detector or absorbed in it. One of the major components of ATLAS hadronic calorimetry is Tile Hadronic Calorimeter (Tilecal) [1, 2].

For each cell of Tilecal the electromagnetic (EM) scale calibration constant converting the calorimeter signals, measured as electric charge in pC, to the energy deposited by measured electrons, which produced the signals, must be determined. The Tilecal EM scale calibration has already been described in Ref [3], but our understanding of the calibration systems continues to improve (see Section 1.2). The use of the charge injection system (CIS) was improved with non-linear corrections for low gain ADCs of the Tilecal channels [4]. The integral cesium calibration method used in [3] was superseded by an amplitude method which provides response information for individual tiles and fibers (see [5] for instance). At the same time, the Fit Method [6, 7] and pulse shapes used for the energy reconstruction have been verified, which resulted in minor improvements in measurement of noise and a better understanding of systematic effects. The EM scale constants presented in this paper were obtained from a new analysis taking into account the mentioned improvements of CIS and cesium calibration and of the Fit Method.

In order to obtain EM scale calibration constant, 11% of Tilecal modules were exposed to electron, pion and muon test beams of various energies at different geometrical set-ups. In this paper, the EM scale was obtained from analysis of response of over 200 calorimeter cells to electron and muon beams.

In order to study the EM scale variation in detail, dedicated Monte Carlo studies were performed in GEANT 4.8.3 using QGSP physics list and Bertini intranuclear cascade model, [8, 9].

This paper represents a result of a dedicated effort of many people in the Tilecal community. In Section 1 Tilecal and its calibration systems are briefly described, Section 2 refers to the beam tests setup. In Section 3 the overall EM scale factor and the main sources of its variation are discussed. Section 4 describes the dependence of calibration constant on radial depth and in Section 5 obtained results are summarized.

1.1 The Tile Calorimeter

Tilecal is composed of a Long Barrel (LB), and two Extended Barrel (EB) cylindrical structures. Azimuthally, barrel and extended barrels are divided into 64 modules, each spanning an azimuthal angle of $2\pi/64$. Radially it extends from inner radius of 2280 mm to outer one of 4230 mm. It is radially segmented into three layers, which are about 1.5, 4.1 and 1.8 interaction length thick at $\eta = 0$. Each of the Tilecal modules is composed of alternating iron plates (absorber) and scintillating tiles (active material). Tiles are oriented perpendicular to the colliding beams and are radially staggered in depth. The trapezoidal scintillating tiles are read-out by wavelength shifting (WLS) fibers on both sides of the tile into two separate photomultipliers (PMTs) as shown in Fig. 1.

The read-out cells are formed by grouping the fibers to individual PMTs. Cells are organized in towers with a given pseudorapidity[1)]. The resulting granularity is: $\Delta\eta \times \Delta\Phi = 0.1 \times 0.1$ (0.2×0.1 in the last radial layer). The layout of the readout cell geometry is shown in Fig. 2. There are 11 transverse rows of tiles (tile rows) in a module. The tile rows are numbered from inner to outer radius. The calorimeter compartments of LB and EB modules are composed of various tile rows shown in Table 1. The Inter-Tilecal Calorimeter (ITC) cells C10 contain tile rows 7-9 and cells D4 contain tile rows 10-11. The height of the tile in radial direction is 97 mm for tile rows 1-3, 127 mm for tile rows 4-6, 147 mm for tile rows 7-9 and 187 mm for tile rows 10 and 11.

[1)] The pseudorapidity η is defined as $\eta = -\ln\tan(\theta/2)$, where the polar angle θ is the angle from the beam axis.

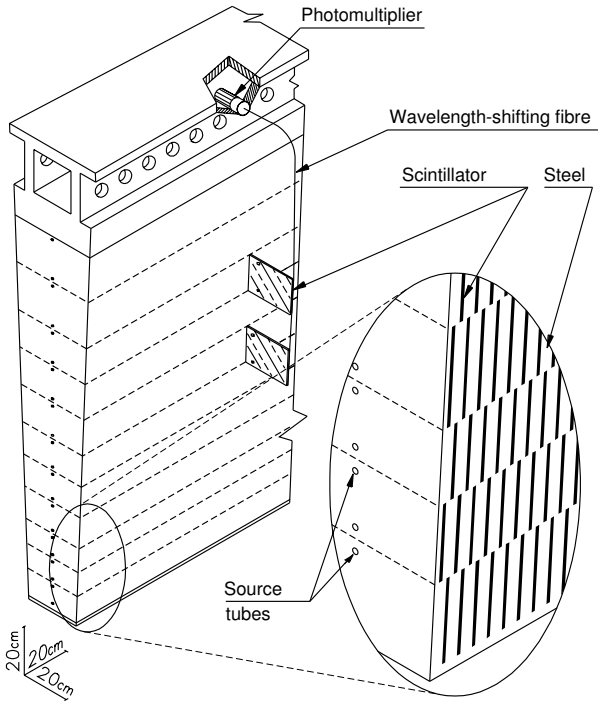

Figure 1: Tilecal module structure and optical read-out elements. The various components of the optical readout, namely the tiles, the fibers and the photomultipliers, are shown. The position of tubes for the cesium source calibration are also shown near the outer edge of each of the eleven tile rows.

Compartment	Long barrel	Extended barrel
A	1-3	1-3
BC	4-9	4-7
D	10-11	8-11

Table 1: The tile rows contained in various LB and EB calorimeter compartments.

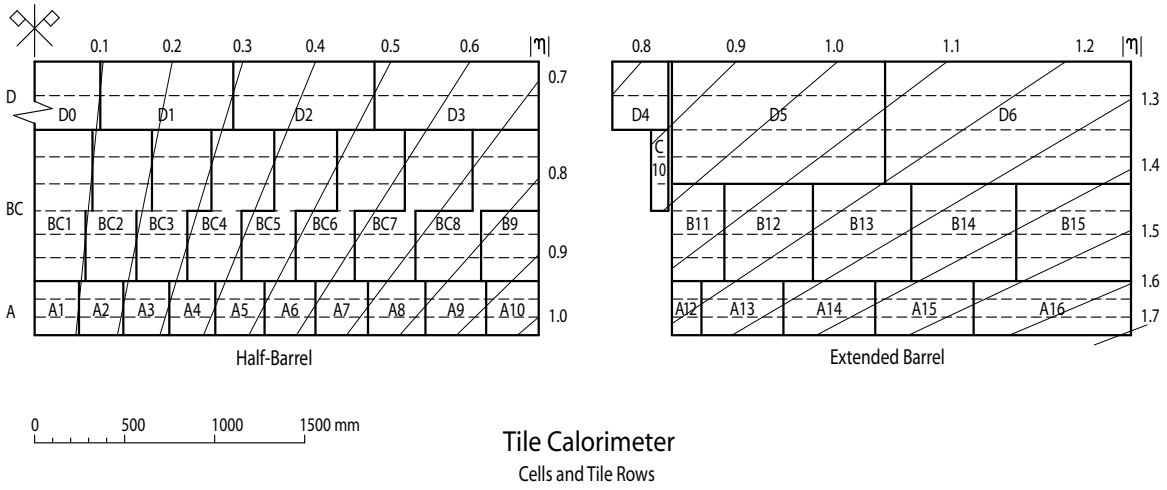

Figure 2: The layout of cells (solid lines) and tile rows (dashed lines) in barrel, extended barrel and ITC (cells D4 and C10) sections of the calorimeter. Also shown are lines of fixed pseudorapidity.

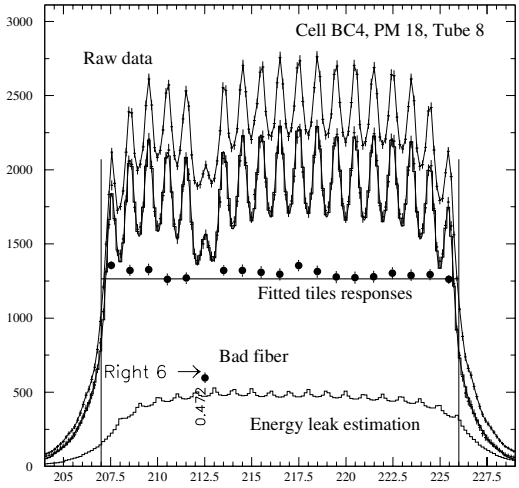

Figure 3: An example of a response of tile row 8 of cell B4 and PMT 18 to the cesium calibration source, as it moves along its path (the distance is indicated on the *x*-axis in cm). The peaks visible in the figure correspond to the Cs source passing through the holes near the edges of individual tiles. The estimate of leak of energy deposited by the Cs source in tile row 8 to other adjacent tile rows of the given cell is also shown. The result for "Raw data" with subtracted leak of energy is shown as the second curve from the top. The relative response of individual tiles is measured with a precision of about 2%. An average cell response is known with 0.3% precision. It is apparent, that for the tile here referred to as "Right 6" the fitted tile response is less than $\approx 50\%$ of the average tile response in the cell. Taken from [10].

1.2 Tilecal Calibration System

The Tilecal calibration system [2] consists of the following components: charge injection system (CIS), cesium system (Cs), laser system and minimum bias (MB) monitoring system. The full potential of MB system can only be exploited with the real data. The calibration constants from laser system were not available for our analysis. The CIS and Cs system were fully operational and their calibration constants were used in our analysis.

The electric charge collected in every Tilecal PMT is passed to bi-gain amplifiers (gain ratio of 64). Both high-gain and low-gain outputs are simultaneously digitized in two 10-bit ADCs. The output of the low-gain (high-gain) channel is used when the value of the signal amplitude measured by the channel is larger (smaller) than ~ 12.5 pC, respectively. During the CIS calibration runs the linearity of response of both the ADCs and the front-end electronics is measured together with the absolute response in ADC counts per pC. A 2% non-linearity in the low gain was measured and corrected.

The cesium system [10] is used as the primary tool to equalize the gain of all calorimeter cells. During cesium calibration runs a radioactive ^{137}Cs source passes through all Tilecal cells, through holes in every scintillating tile and absorber plate. The holes for cesium calibration tubes are located 13 mm from the outer radius edge of the trapezoidal-shaped tiles (independently of the tile size), on its symmetry axis, as shown Fig. 1. The Cs system measures the relative efficiency of the optical read-out chain between every tile in the cell and the associated PMT. A sample scan is shown in Fig. 3. The high-voltage of the PMT is then set to ensure that the average response of all tiles in the cell corresponds to the overall Tilecal average for the given calorimeter compartments.

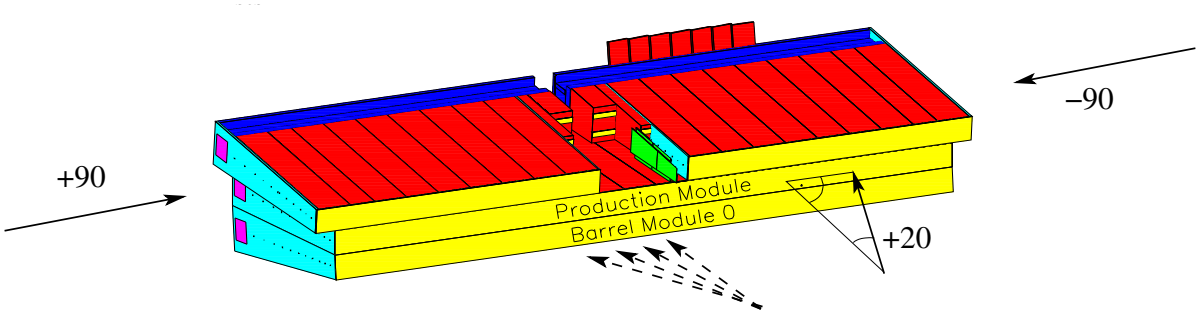

Figure 4: Tile Calorimeter module layout during beam test operation in the H8 area of the CERN SPS. From bottom to top the Module 0, a production barrel module and two extended barrel modules are shown. Approximate beam directions for $\theta = +90^\circ$, $\theta = -90^\circ$, $\theta = +20^\circ$ and η-projective setup (dashed arrows) are shown.

2 Testbeam setup

The calorimeter setup in the H8 area of the CERN SPS is shown in Fig. 4. On a scanning table capable of x, y, θ and ϕ motion, the prototype Module 0 is the lowest in a stack of three modules. The middle layer is a production barrel module, and the top layer is either a pair of production extended barrel modules (as shown in the figure) or another production barrel. Since some data are taken in projective geometry, module orientation is denoted by positive or negative η, with positive η being the beam-right side on the scanning table.

Calibration of each module consists of using the beam in the following geometries:

- Beam incident at the center of the front face of each A cell at $\pm 20^\circ$ from the normal;
- Beam incident at projective angles across the front face of the calorimeters;
- Beam incident at the sides of the calorimeters into the center of each tile row. This is referred to as 90° measurements.

Beam energies for measurements reported in this paper were between 20 and 180 GeV. In general, the beam composition was a mixture of hadrons, muons and electrons. The particle type is identified mainly by using the calorimeter response. A pair of beamline Cerenkov counters assisted in further identification. For beam energies $E_{\mathrm{beam}} \leq 20$ GeV the Cerenkov signal is used to improve electron/hadron separation, for positively charged beams ($50-180$ GeV) it is used for pion/proton separation. Beam transverse position is measured with two x-y wire chambers upstream of the calorimeter.

3 Electromagnetic scale

In this section the Tilecal EM scale calibration constant is obtained from an analysis of the Tilecal response to electron test beams. We will also discuss the precision of the obtained EM scale and its dependence on the pseudorapidity of the beam. In all cases shown below the channel energy was calculated using the Fit Method [6, 7], amplitude cesium calibration method [5] and CIS calibration including the non-linear corrections for low-gain ADCs [4].

The response of calorimeter modules to electron beams is defined as the ratio of the charge collected in analyzed cells of the calorimeter module to the electron beam energy. The charge collected in one cell is equal to the sum of charges collected by the two PMTs reading-out the cell.No corrections for dead material were taken into account.

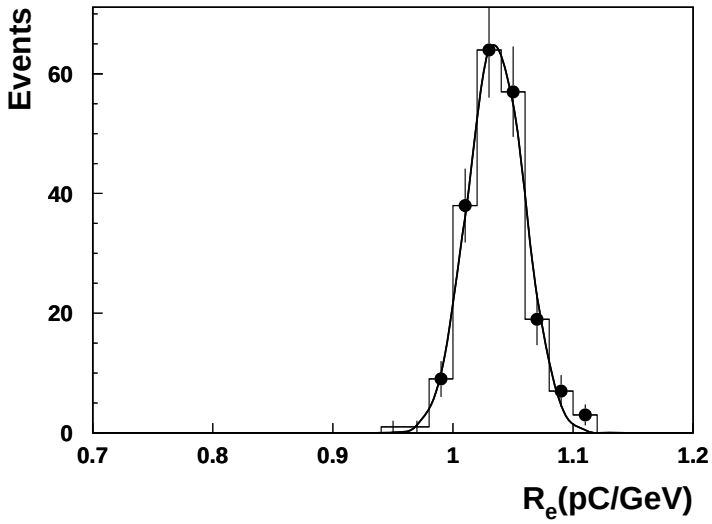

Figure 5: The cell response of electrons at the angle $\theta = \pm 20^\circ$ (Mean = 1.050 ± 0.003 pC/GeV, RMS = $2.4 \pm 0.1\%$), with one entry for each A-cell measured. The plot contains data taken at 20, 50, 100 and 180 GeV electron beam energies.

3.1 Electromagnetic scale calibration constant from electron runs

In order to obtain the Tilecal EM scale calibration constant the response of all A cells of three long barrel modules and five extended barrel modules to electron beams was studied[2)]. The beams entered the modules at $\theta = \pm 20^\circ$, having energies of 20, 50, 100 and 180 GeV. Only runs with all PMTs working were included in the analysis.

A distribution of all obtained responses of over 200 calorimeter cells is presented in Fig. 5. The mean value of this distribution is 1.050 ± 0.003 pC/GeV and is taken as the Tilecal electromagnetic scale. The RMS spread of the measurements is $2.4 \pm 0.1\%$.

3.2 EM scale variation

As was shown in the preceding section 3.1, the EM scale calibration constant of Tilecal is known with RMS spread of $2.4 \pm 0.1\%$. In this section we will discuss the sources of this variation: a variation of tile-to-phototube optical read-out efficiency, an effect of fast and slow read-out electronics and a dependence of the EM scale calibration constant on pseudorapidity and energy.

3.2.1 Variation of tile-to-phototube optical read-out efficiency

Each Tile calorimeter cell is a set of scintillator tiles connected by optical fibers to two phototubes (Section 2). Between the fibers and the phototubes there are light mixers to spread the light from the optical fiber on the surface of the photo-cathode of the PMT and thus minimize the influence of the photo-cathode non-uniformity. The optical read-out efficiency between each tile and each of the two associated phototubes is measured by the cesium calibration system (see Section 1.2). Variations of this efficiency arise from: non-uniformity inside a tile, tile-to-tile fluctuations, tile-to-fiber coupling, fiber-to-fiber fluctuations, variations of the response across the PMT photo-cathode (with the light mixer in

[2)] The following modules were analyzed in this case: extended barrel modules ANL-23, ANL-30, ANL-44, IFA-27 and IFA-42; long barrel modules JINR-12, JINR-27 and JINR-55.

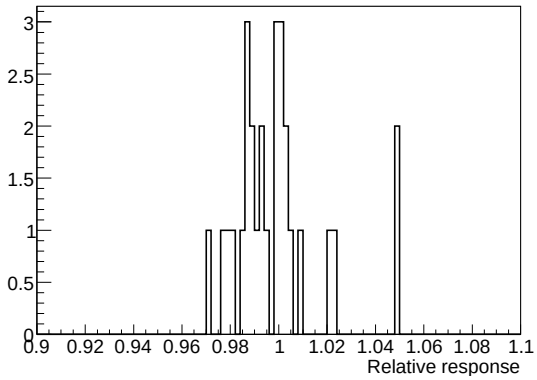

Figure 6: Simulated mean response at 28 different impact points for 180 GeV electrons incident on a barrel module at $\theta = 20^\circ$. The RMS spread of the means is $1.8 \pm 0.2\%$. The response is normalized to the case when no Cs amplitude weights are introduced (that is the standard setup in the simulation).

front), and fluctuations inside a cell due to the fact that more than one tile is read out by the same optical fiber.

The cesium measurement showed that the distribution of the tile-to-phototube optical read-out efficiency has an RMS spread of $\approx 5\%$, [11]. An electron beam at $\theta = 20^\circ$ crosses only a part of the tiles of a given cell and the response of the cell depends on the optical fluctuations of the hit region. Could these optical fluctuations explain partially the variation of EM calibration constant? In order to answer this question a dedicated Monte Carlo study was performed.

The relative signals from each tile obtained from the Cs source measurements were introduced in the Monte Carlo simulation of the testbeam setup for every single tile-to-phototube coupling. The weights are based on Cs amplitude signal as measured during Cs scan of a real barrel module JINR55. The weights are calculated as follows:

$$w_{Cs}(tile, PMT) = \frac{Cs_{Amp}(tile, PMT)}{\text{average over tiles in the cell}(Cs_{Amp}(tile, PMT))} \quad (1)$$

After introducing these weights in the MC simulations, electron beams ranging in energy from 10 to 180 GeV were simulated in the barrel module at $\theta = 20^\circ$ and 28 different impact points. The RMS spread of the mean response was $1.8 \pm 0.2\%$. Fig. 6 shows an example for 180 GeV electrons. Similar RMS spread was obtained with other electron energies.

In the real testbeam measurement, it is not possible to correct for differences of optical tile-to-phototube couplings as the mutual position of modules at the scanning table and the beam is not known with sufficient precision and the shape of electron showers fluctuates event to event. Therefore the spread of tile-to-phototube optical couplings is present also in the real data. In the case of barrel module JINR55 and 180 GeV electron runs at $\theta = 20^\circ$ the uniformity of cells at $\eta < 0$ is 1.8%, $\eta > 0$ is 2.0% and the uniformity of all cells exposed to the electron beam is 2.2%.[3)] This is in a good agreement with the result obtained in the simulation.

In the real data few other cases illustrating this phenomenon were observed. In these cases a larger RMS spread of response with position has been observed and traced to poor tile-to-phototube couplings using information from the Cs scans.

[3)] Part of the difference between the two sides ($\eta < 0$ and $\eta > 0$) comes from the fact, that integrators in testbeam were not calibrated. As described in Section 3.2.4, the differences are $\sim 0.5\%$.

We conclude, that the spread of tile-to-phototube optical couplings is the main factor determining the 2.4% RMS spread in calorimeter EM scale calibration constant.

3.2.2 EM scale energy dependence

The electron linearity has also been investigated in several beam test periods, where electron beams at various energies impinged the Tilecal modules at a given angle. Since electrons produce compact EM showers, it is expected that the tile-to-tile differences (see Section 3.2.1) deteriorate the linearity as well.

The experimental results are shown in Fig. 7, left panel. The presented data include three barrel modules with electrons entering at $\eta = -0.35$ ($\theta = 20^\circ$).

The impact of the tile-to-tile differences has been studied with special MC, where the tile-to-phototube optical coupling has been introduced according to the Cs-scan data from a real Tilecal module. The JINR-55 barrel module has been chosen for this exercise. The MC electron linearity is displayed in Fig. 7 (right panel) for five different impact points spaced by 1 period (18 mm) along z-axis. The obtained MC results demonstrate that:

- Even with no tile-to-phototube variations there would be a small internal non-linearity of the EM response at the level of 0.5% between 10 GeV and 180 GeV. This is mainly due to the 1 cm thick passive front-plate placed in front of the active part of the calorimeter.
- The tile-to-tile differences have a significant impact on the electron linearity. If the beam was shot in the same impact point for all energies, the non-linearity would be within 2%. If we allow the beam impact point to change energy-to-energy, the non-linearity can increase to about 3%.

In the Tilecal standalone testbeam, the beam was tuned to a given energy and then the table was positioned at many different impact angles and points. Afterwords, the beam was tuned for another energy. Since the precision of the table position along z-axis is limited (order of cm), the table position was very likely different for different energies.

We conclude that the electron non-linearity observed in the testbeam can be mostly explained with the tile-to-tile differences and the variation of the impact point between various test beam measurements. This effect dominates the non-uniformities of the calorimeter response to electrons.

3.2.3 Effect of fast read-out electronics

The calorimeter front-end fast read-out electronics is calibrated by a dedicated charge injection system, described in detail in [4]. It is important to recall one of the main conclusions of this study that the systematic uncertainty of the CIS calibration including the differential ADC non-linearity is less than 0.7% for measurements with a single channel. This uncertainty is a few percent for charges below 1 pC and in the region from 10 to 50 pC, corresponding to the lower limit of the range of the high-gain and low-gain channels.

When calculating the response of the calorimeter to electron beams, signals from several read-out channels are summed to cover the whole electromagnetic shower. The resulting systematic uncertainty due to systematic uncertainty of CIS calibration constants is then smaller than the one of a single channel as shown in Fig. 8, [4].

The uncertainty in the mean response to electrons caused by a systematic error of CIS is less than 1% over the range of energies from 20 to 180 GeV. In the case of jets in ATLAS this uncertainty is expected to be even smaller, since signal will be collected from a larger number of channels.

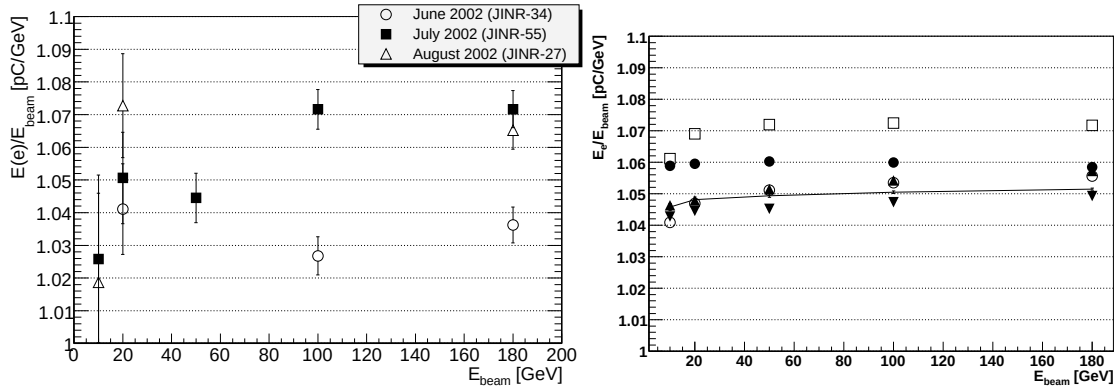

Figure 7: The electron linearity at $\eta = -0.35$. Left panel: linearity measured in three different barrel modules. Right panel: linearity determined with MC, simulating also individual tile-to-phototube couplings for each tile/fiber as observed in a real module. Different symbols correspond to five different impact points, spaced by 1 period. The difference of response for various impact points is caused by different tile-to-phototube weights of tiles hit by the electron shower at the given impact points. The solid black line corresponds to the case with all tile-to-phototube weights equal to 1.00 (that is the standard setup in the simulation).

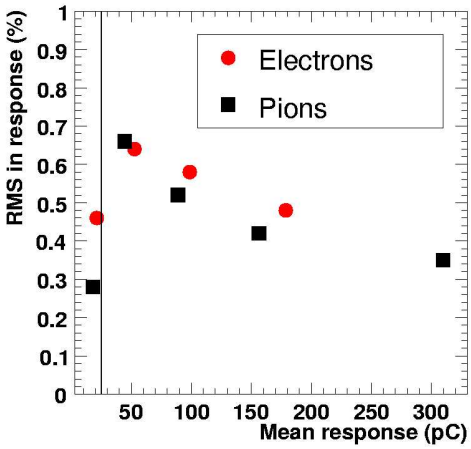

Figure 8: Expected systematic uncertainty (caused by the uncertainties of the CIS calibration) on the mean response for test beam measurements with electrons and pions as a function of the total measured charge. The vertical line indicates the approximate position of the gain switch when the signal is read out by two channels. Taken from [4].

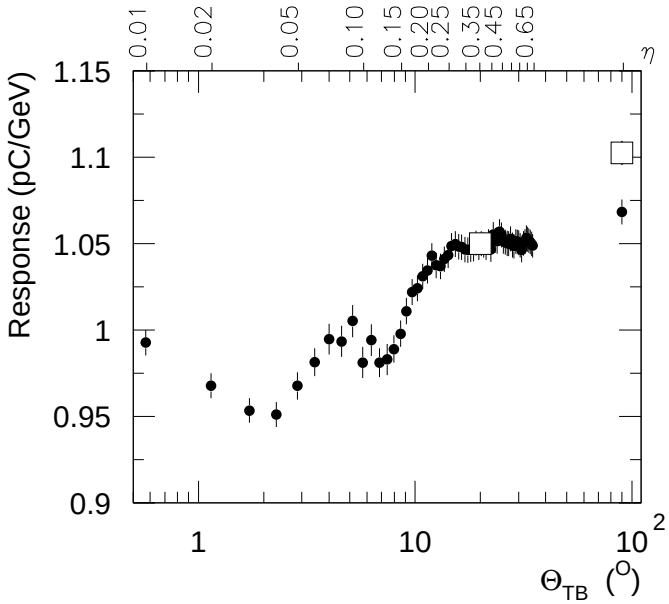

Figure 9: The dependence of EM scale calibration constant on θ with 20 GeV electron runs. Tilecal experimental data for $\theta = 20^\circ$ (three LB and five EB modules analyzed) and $\theta = 90^\circ$ (three LB modules analyzed) shown as open squares. Monte Carlo simulation results (full circles) are normalized to data at $\theta = 20^\circ$. Variation of EM scale calibration constant of 10% is observed within the considered range of angles. The reason the $\theta = 90^\circ$ experimental data shows $\sim 3\%$ higher value than the simulation is the non-uniformity of the tile response over its surface and is qualitatively understood, as described in the text.

3.2.4 Effect of slow read-out electronics

The calorimeter cells are not only read out by fast electronics with a sampling frequency of 40 MHz to obtain the physics collision data, but they are also read out by slow read-out electronics for the purpose of minimum bias monitoring and cesium calibration.

For each calorimeter channel there is one charge integrator dedicated for this purpose. The calibration of the integrator gain thus influences the precision of the cesium calibration constants. In the case of data presented in this paper, the integrator calibration constants were not taken into account during cesium calibration scans. Nevertheless it was measured, that the integrator calibration constants have RMS spread of 0.5% [12, 13], therefore their influence on the EM scale calibration constant is very small.

In ATLAS, the integrator calibration constants will be used for the cesium scans and that can improve the EM scale calibration constant precision from 2.4% to 2.3%.

3.2.5 EM calibration constant versus pseudorapidity

The EM scale calibration constant presented in section 3.1 is based on an analysis of electron runs at $\theta = 20^\circ$. However, as particles enter calorimeter modules under all possible angles, the dependence of EM scale calibration constant on θ was also studied.

The following sources of data were used: real data from 20 GeV Tilecal electron runs (three LB and five EB modules analyzed with $\theta = 20^\circ$, three LB modules analyzed with $\theta = 90^\circ$) and MC simulation of 20 GeV electron runs. The covered range of θ is 0° – 90° for simulation and 20° and 90° for data. The result of this analysis is depicted in Fig. 9.

The response to electron beams increases with the incident angle θ by 10% between $\theta = 0^\circ$ and $\theta = 90^\circ$ and can be qualitatively understood as as due to the periodic tile/iron structure of the calorimeter, but it was not studied quantitatively. It is also apparent that in the region $\theta = 15^\circ$ to $\theta = 35^\circ$ the response to electrons is flat within the errors. The ratio of the response measured at $\theta = 90^\circ$ and $\theta = 20^\circ$ is 1.06 in experimental data, while in the simulation it is 1.02. The higher value of this ratio observed in the data can be qualitatively explained by the fact, that the response of tile center, hit by beams at $\theta = 90^\circ$, is $\sim 3.5\%$ higher[4)] than the tile response averaged over its surface due to the optical properties of the trapezoidal shaped tiles, [14]. The electron beams with $\theta = \pm 90^\circ$ deposit $\sim 95\%$ of energy within the tile row they traverse. In the case $\theta < 90^\circ$ the beam hits are distributed over a larger area of the tile surface, so a decrease of the signal response with respect to the $\theta = 90^\circ$ beams is expected. The tile non-uniformity is not simulated in the current Monte Carlo simulation.

The angular dependence of Tilecal response was also measured at the EM scale with hadron beams. For pion beams the angular dependence is negligible, once the longitudinal leakage is corrected for, see Fig. 10. The longitudinal leakage corrections are based on the shower shape measurement performed separately for pion and protons [15]. The actual corrections used reflect the expected pion-to-proton ratio in the beam since no pion-proton separation was possible in this dataset.

A Monte Carlo simulation with longitudinal leakage correction also predicts a very small angular dependence of the response, for pseudorapidities $\eta > 0.2$ the response changes by less than 0.5%. Both for data and MC simulation the signal was collected from 3×3 towers (a region with $\eta \times \phi = 0.3 \times 0.3$).

Even more detailed pseudorapidity scan was investigated with barrel module zero [16], the results are similar. We conclude that angular dependence of the EM scale can be neglected. This is especially true in the ATLAS configuration where hadronic leakage is smaller and only hadrons will be detected.

4 Calibration constant versus radial depth

The electron beams used for setting the calorimeter EM scale deposit most of their energy in the A compartment of calorimeter modules. In this section we focus on the question, whether the cells in BC and D compartments are properly calibrated at the EM scale after the cesium calibration. This was studied using muon and electron beams.

4.1 Corrections to the Cs source calibration using muons at 90°

Muons entering the calorimeter modules at $\pm 90^\circ$ along the centers of the tiles are used to study the uniformity of the individual cell response and to test, whether the EM scale is preserved also in the second and third calorimeter compartments, where most of the cells can not be reached by the electron beams. As we will show in this Section, additional correction factors to the Cs source calibration, here referred to as the particle/Cs correction factors, are needed to preserve the EM scale in all calorimeter compartments.

The difference between the calorimeter response to particles and to Cs source originates in the non-uniformity of the individual tile response across its surface. The pipes carrying the Cs source run through holes in the tiles near their outer edges. A dedicated measurement showed[5)] that more than 90% of light produced when the Cs source traverses the tile is collected from a circle around the hole with a radius

[4)] More details are given in Section 4.1.

[5)] Cs decays by a pure beta decay to a metastable nuclear isomer of barium Ba-137m, which consequently emits 662 keV photons. An absorption length for such photon in iron is ~ 1.9 cm, while in scintillator it is more than one order of magnitude larger. Most of the photons thus interacts in the iron close to the Cs pipe by Compton's scattering and photoelectric effect, ejecting electrons into the scintillator, where the detected light is produced. The size of the area, where this light is produced was measured in [17].

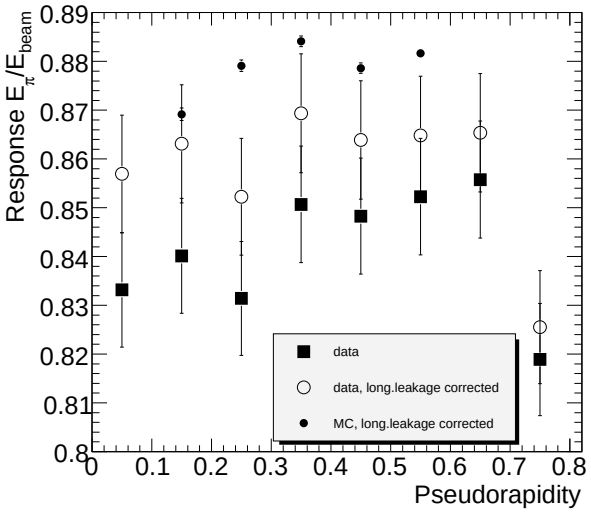

Figure 10: An example of the Tilecal response to 180 GeV hadrons (pions and protons) as a function of pseudorapidity η (black squares). After correcting for longitudinal leakage (open circles), the response does not depend on η significantly (the point at $\eta = 0.75$ already suffers from side leakage). Superimposed are MC results including longitudinal leakage correction (small full circles). The MC data was simulated only for five values of pseudorapidity in the range of 0.15 to 0.55. MC also predicts only small angular dependence of the response, changes are less than 0.5% for $\eta > 0.2$. Particle/Cs correction factors were applied to data, see Section 4.1 for explanation. The absolute difference between data and MC simulation is approximately 1%.

of ~ 2.5 cm. The distance between this Cs "calibration circle" and the center of each tile increases with the size of the tile and hence with radial position in the calorimeter. The associated correction factor is discussed below.

The response to muons was studied with a muon beam directed along the center of each tile row. Since showers induced by particles entering at projective angles spread almost uniformly over the tile surface, a first question is whether the response at the center is representative of an average response over the full tile. It has been shown in a dedicated measurement using ^{90}Sr and ^{137}Cs sources that the response of a circle of 2.5 cm radius located in the center of the tile is 3.5% higher than the response averaged over the whole tile surface, [14], as shown in Fig. 11. In this measurement two sets of tiles were used, each consisting of three tiles of size 1, three tiles of size 11 and one tile for each size from 2 to 10. The dependence of this response ratio on the tile size for the sample of 30 tiles in two sets of 15 is shown to be flat in Fig. 12. The tile center response thus represents the tile response averaged over its whole surface. Therefore, particles traversing the calorimeter along the centers of each tile row provide a tool suitable for evaluating the particle/Cs correction.

Most of the tested modules were exposed to muon beams at $\theta = 90^\circ$ with energy of 180 GeV. The muon signal scales primarily with the cell length along the muon path. However, this is true only for the mean value over the full signal spectrum. Such a quantity is very sensitive to high energy tails of the muon signal spectrum, caused by radiative processes. Therefore the mean value of the muon energy loss spectrum truncated at 97.5% of the total number of entries, here referred to as TM97.5, was adopted as the definition of the calorimeter response to muons. High-energy muons also lose energy via radiative processes that are strongly energy dependent. This leads to a 2.5% decrease in the muon $\mathrm{d}E/\mathrm{d}x$ over the 6 m path through the calorimeter module [18].

To avoid the systematic uncertainties associated with muon radiative energy losses and with the

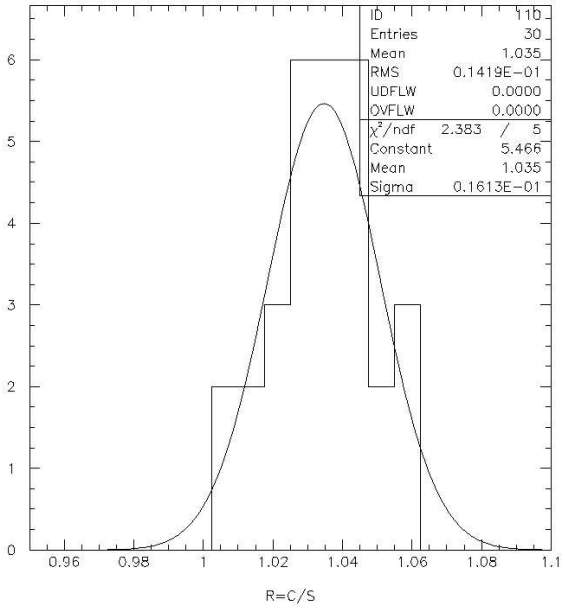

Figure 11: A ratio of the response to Sr source illuminating a circle of 2.5 cm radius located in the center of the tile to the response of the whole surface. A sample of 30 tiles was used; six tiles of size 1 and 11 and two tiles of each size for tile sizes 2 to 10. Taken from [14].

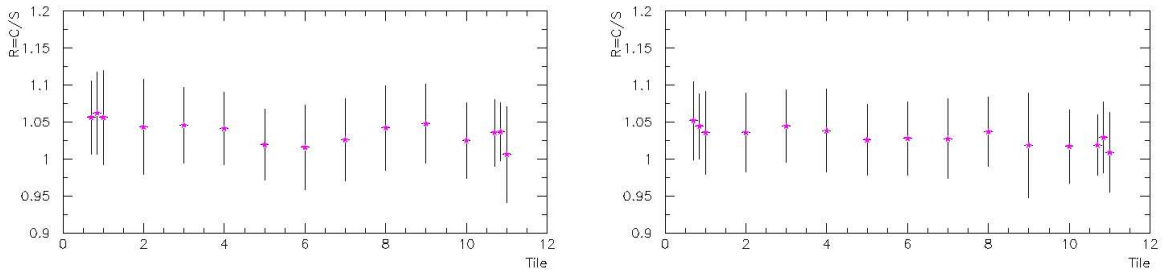

Figure 12: A ratio of the response to Sr source illuminating a circle of 2.5 cm radius located in the center of the tile to the response of the whole surface as a function of the tile row number. Two samples of tiles were measured and the reproducibility is shown. Taken from [14].

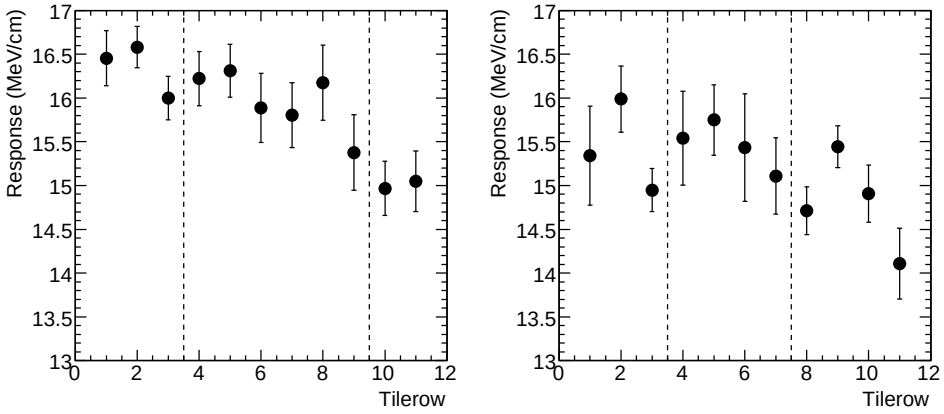

Figure 13: The muon response summed over the full calorimeter module length in the 90° configuration, averaged over all analyzed modules and divided be the muon path length (560 cm in barrel and 255.5 cm in extended barrel module, end-plates excluded). Results for barrel modules (left) and extended barrel modules (right) are presented. The dashed lines show the edges of radial compartments (A, BC and D from left to right), for which the particle/Cs correction factors are computed. The fact that path length normalized response to muons is in average lower in EB than in LB is understood and confirmed by Monte Carlo studies. Details are given in the text.

dependence of truncated mean on the muon path length, the muon signal was summed over the full length of the calorimeter module. The total muon signal is measured in every tile row. The response of Tilecal modules to muon beams at $\theta = 90^\circ$ is presented in Fig. 13. The charge-to-energy conversion was done by dividing the measured charge by the conversion factor of 1.10 pC/GeV obtained from the response to electrons at $\theta = 90^\circ$ (compare with Fig. 9 and Fig. 14, the response of A compartment of the modules) and multiplying by the ratio of electron and muon responses $e/\mu = 0.91$, [19].

After the gain of all cells in the calorimeter is equalized with Cs calibration, the muon response depends on the tile row number. This feature is partially corrected by applying correction factors in individual radial compartments.[6)] The correction in the radial compartment A is set to one, in order to preserve the EM scale as determined with electrons at 20°. The particle/Cs correction factors for the second and third radial compartment are the ratios of the mean responses of the tile rows of the first compartment to the mean muon responses of the tile rows of second and third compartment, respectively.

The muon data were analyzed in both barrel and extended barrel modules. The pattern observed in extended barrel modules is basically the same as in barrel modules (see Fig.13), but the correction factors differ mainly because of different radial segmentation. The second radial compartment in barrel modules is composed of six tile rows, read-out by optical fibers of four different lengths and the third radial compartment is composed of two tile rows, read-out by optical fibers of two different lengths. In extended barrel modules, four tile rows (read-out by optical fibers of two different lengths) constitute both second and third radial compartment (see Section 1.1). The correction factors are averaged over all modules analyzed (five long barrel modules and six extended barrel modules). Their values are listed in Table 2. In addition to the correction factors listed in Table 2, other correction factors are needed for ITC cells and long barrel cell B9[7)]. These correction factors are listed in Table 3 and were calculated

[6)] The individual tile row correction cannot be applied for beams entering at projective pseudorapidities, since every PMT collects the signal from several tile rows in the given cell.

[7)] ITC cells and long barrel cell B9 are composed of different tile rows than the standard calorimeter compartments. ITC cell C10 involves tile rows 7-9, ITC cell D4 involves tile rows 10 and 11, long barrel cell B9 involves tile rows 4-6.

Compartment	Barrel	Extended barrel
A	1.000	1.000
BC	1.025 ± 0.002	1.009 ± 0.005
D	1.088 ± 0.005	1.055 ± 0.003

Table 2: The particle/Cs correction factors for the middle (BC) and the last (D) calorimeter compartment to keep the EM scale equalized in all cells in a module. Values are averaged over several modules and statistical errors are shown.

Cell	particle/Cs weight
ITC cell C10	1.036 ± 0.008
ITC cell D4	1.088 ± 0.005
Barrel cell B9	1.014 ± 0.006

Table 3: The particle/Cs correction factors for ITC cells C10 and D4 and long barrel cell B9 to keep EM scale equalized in all cells in a module. Values are averaged over several modules and statistical errors are shown.

assuming the same response to muon beams in ITC tile rows as in corresponding extended barrel tile rows.

The response to muons normalized by path length, as shown in Fig. 13, is in average lower for EB modules than for LB modules. This has two reasons: the nonlinearity of TM97.5 signal calculation method (the value of TM97.5 does not scale perfectly linearly with the muon path length in the cell) and the fact, that the muon energy lost by bremsstrahlung and pair production in the first module cell (at the beginning of the muon path through the module) is deposited partially in subsequent cells, so the first cell the muon enters has a smaller response. This effect is relatively less apparent in longer LB modules. The difference between LB and EB modules muon response was confirmed by a Monte Carlo study with a precision better than 1%.

The response variation for 180 GeV electron beams at 90° is shown in Fig. 14. It exhibits a similar variation to that shown for muons in Fig. 13. However these electron runs were not used for determining the precise dependence of EM scale on radius, as they deposit most of their energy in the first calorimeter cells they enter and do not traverse the whole module as muon beams do.

We recall here the explanation, why the second and third compartments are under-calibrated after Cs calibration and calibrating the first compartment at EM scale. Detailed measurements of the response of tiles to collimated Sr β-source have shown, that there is a systematic decrease of the tile signal collection with position of the source along the tile radius of 1 %/cm to 2 %/cm from the outer edge to the inner edge of the trapezoidal tiles, [14]. We remind, that Cs scans excite tiles near the outer radius holes, which have their center always placed 13.5 mm from the tile edge; while particles from $\theta = 90^\circ$ beams enter the center of tiles. As an example, in tiles of tile row 11 (included in the third compartment), the distance between the tile center and the Cs hole is 80 mm, while in tiles of tile row 1 (belonging to the first compartment), this value is only 35 mm. This distance difference and the 1 %/cm to 2 %/cm signal decrease in the radial direction of the tile causes an under-calibration of tile 11 (in compartment D) with respect to tile 1 (in compartment A) of 4-8%. Similar considerations are valid for other tile sizes with under-calibration increasing with the tile size, i.e. for tiles located at larger radius. Early Tilecal prototype modules did not have this dependence on radius because scintillators in all the tile rows had the same radial depth of 10 cm, [2].

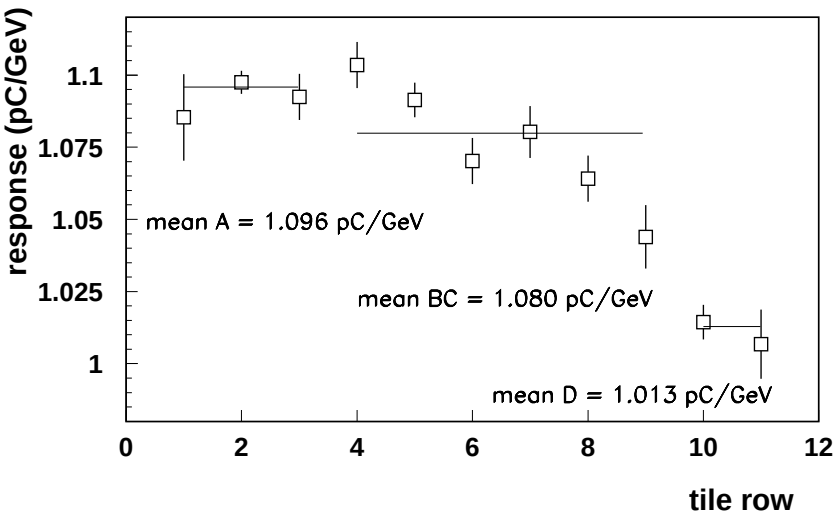

Figure 14: The response of calorimeter barrel modules to electron beams at $\theta = \pm 90^{\circ}$, averaged over three modules (JINR12, JINR27 and JINR55). Results are shown after the normal Cs calibration with no additional correction factor associated with the tile size. A similar response dependence on tile row number is observed also with muon beams.

4.2 Particle/Cs correction factors and eta-projective muons

In this section we will show a comparison of particle/Cs correction factors obtained from muons at 90° and eta-projective muons. We will also show an overall uniformity of response of measured Tilecal modules to eta-projective muon beams, when the particle/Cs correction factors listed in Table 2 are used in the analysis.

4.2.1 Comparison of particle/Cs correction factors from muons at 90° and eta-projective muons

The particle/Cs correction factors listed in Table 2 and Table 3 were obtained from the analysis of the calorimeter response to muon beams at $\theta = 90^{\circ}$. The particle/Cs correction factors can also be obtained from an analysis of the calorimeter response to eta-projective muons, which corresponds to the geometrical setup in the ATLAS detector. In this section we will present the particle/Cs correction factors for the barrel modules obtained from eta-projective muon beams [20], discuss the systematic uncertainty of these particle/Cs correction factors and compare them with the correction factors listed in Table 2.

When muon enters the calorimeter module, it looses energy by ionization and radiative processes. While in the case of ionization process muon energy is lost and deposited in the same position; in the case of radiative processes muon energy is deposited in a volume downstream from the position of the actual energy loss, as described in detail in Refs. [21, 22]. As a consequence muon $\mathrm{d}E/\mathrm{d}x$ in the first cell the beam enters is smaller by up to 10-20% than in the following cells, depending on the muon energy and the first cell length [22]. This effect is referred to as the "first cell effect".

When calculating particle/Cs correction factors from the calorimeter response to eta-projective muon beams, the real data must be corrected for the "first cell effect" by means of the Monte Carlo simulation. This is fully possible only if there is a sufficient agreement between the spectrum shapes of muon energy detected in compartments of the calorimeter towers in both real data and the Monte Carlo. With the current Monte Carlo the agreement of the muon energy spectra in its low energy tail was not sufficient.

Compartment	Barrel
A	1.000
BC	1.029 ± 0.029
D	1.092 ± 0.051

Table 4: The particle/Cs correction factors obtained from analysis of barrel module JINR55 response to muon eta-projective beams, averaged over analyzed towers. The "first cell effect" correction based on Monte Carlo simulation is included. The muon signal was calculated with TM15 method described in the text. See text for details.

In order to calculate the muon signal a method less sensitive to low energy spectrum tails, defined in [21], was used. In this method, here referred to as TM15, the muon signal was calculated as a mean value from the muon response energy spectrum truncated at MOP $-\,1\sigma$ and MOP $+\,5\sigma$, where MOP and σ are the most probable value and the standard deviation of the Gauss-Landau convolution fitted to the spectrum, [23].

In order to calculate the particle/Cs correction factors from eta-projective muon beams the responses of individual compartments of calorimeter towers obtained from the analysis of barrel module JINR55 were divided by the corresponding values obtained from the Monte Carlo. In the current Monte Carlo simulation the propagation of light through individual tiles is not described and the tiles are defined to have perfectly uniform response. Thus the main difference between the Monte Carlo and real data are the particle/Cs correction factors. The resulting ratios correspond to responses of individual compartments of calorimeter towers corrected for "the first cell effect"[8)] and were used for the calculation of the particle/Cs correction factors that are listed in Table 4.

We would like to point out, that the errors of particle/Cs correction factors listed in Table 4 are much larger, than the errors of the particle/Cs correction factors listed in Table 2. This has several sources. Firstly, the response of the calorimeter modules to eta-projective muon beams is very sensitive to the precise value of pseudorapidity. In [24] the response of a barrel module in a Monte Carlo simulation to the 150 GeV muon beams with pseudorapidities $\eta = 0.438$ and $\eta = 0.441$ was studied. It was shown, that although the only difference in both cases was only a small shift of $\Delta\eta = 0.003$, or ≈ 4 mm, the deposited energies differed significantly, 4% for the truncated mean TM15. Secondly, the path of eta-projective beam through the calorimeter module is shorter than in the case of beams at 90° and the length of this path is more sensitive to the position of the module with respect to the beam, which is known with a limited precision (~ 1 cm). Finally, a smaller number of modules was analyzed in the case of eta-projective muon beams compared to muon beams at 90°.

We conclude that the particle/Cs correction factors listed in Table 4 agree within errors with the values obtained from muon beams at 90° and presented in Table 2. However because of the mentioned limitations in the accuracy of the particle/Cs correction factors listed in Table 4, it is preferable to use those from muon beams at 90°.

The response of Tilecal module to eta-projective muon beams was also analyzed in [21]. The particle/Cs correction factors in Table 2 are compatible with the results in [21], taken into account, that in the case of [21] LAr calorimeter was placed in front of the Tilecal module and an older Cs integral calibration method was used, with which the response of D-compartment of the Tilecal module was incorrectly 4% higher than our current Cs calibration.

[8)] The "first cell effect" is canceled in these ratios. We recall that due to this effect the muon $\mathrm{d}E/\mathrm{d}x$ in the first cell the beam enters is smaller by up to 10-20% than in the following cells.

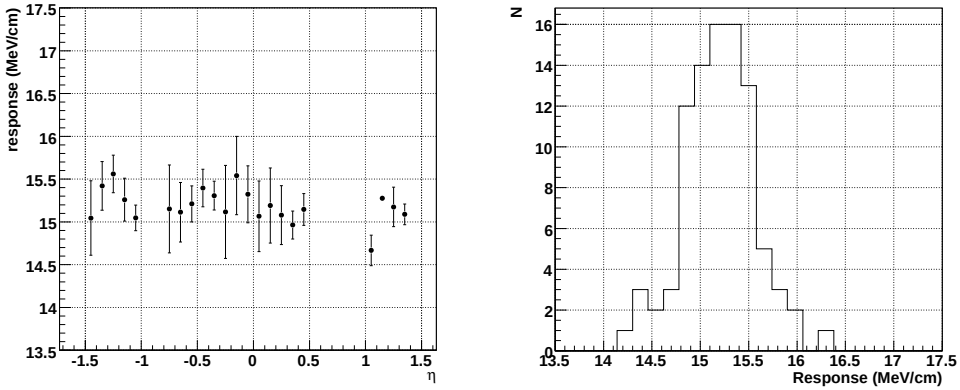

(a) Mean response to eta-projective muons

(b) Distribution of Tile tower response

Figure 15: Tilecal response to 180 GeV eta-projective testbeam muons averaged over all analyzed modules (3 LB modules and 6 EB modules). Response vs. pseudorapidity (a) and summarized for all 91 analyzed Tilecal towers (b) with mean value 15.2 MeV/cm and uniformity of 2.5%. Barrel data points cover $-0.75 < \eta < 0.45$, extended barrel point cover $|\eta| > 1.0$.

4.2.2 Applying particle/Cs correction factors to eta-projective muons

In this section the particle/Cs correction factors obtained in Section 4.1 from 90° muon runs were used in the analysis of eta-projective muon beams with energy of 180 GeV (eta-projective beams correspond to the geometry of the real ATLAS setup). The energy measured in the cells of various calorimeter compartments was multiplied by the correction factors presented in Table 2.

In total six extended barrel modules (4.7% of all EB modules) and three barrel modules (4.7% of all LB modules) were analyzed. The energy measured in every calorimeter tower was normalized to the mean path length of muon traversing the calorimeter at each given pseudorapidity. The dependence of path length normalized responses averaged over analyzed modules on η and distribution of this response for all analyzed runs are depicted in Fig. 15.

The resulting mean value of the response is 15.2 MeV/cm with an uniformity of 2.5%. The muon signal and noise in the tower are well separated with signal-to-noise ratio $(S/N) \approx 44$.

5 Summary and conclusions

We have shown that the overall EM scale calibration constant in Tilecal (1.05 pC/GeV) is known with an RMS spread of 2.4 ± 0.1%, mainly limited by variations in the tile-to-phototube optical coupling efficiencies. The sources of the EM scale variation were discussed in detail.

It was also shown, that the procedure of keeping all Tilecal cells on the same EM scale requires particle/cesium correction weights. In the second compartment the measured signals need to by multiplied by 1.025 ± 0.002 and 1.009 ± 0.005 for long barrel and extended barrel, respectively. For the third compartment these weights are 1.088 ± 0.005 and 1.055 ± 0.003 for long barrel and extended barrel, respectively. The particle/cesium correction weights for ITC cells C10 and D4 are 1.036 ± 0.008 and 1.088 ± 0.005, respectively, and for barrel cell B9 the value 1.014 ± 0.006 was obtained.

In near future additional cesium calibration corrections will be needed in the ATLAS pit in order to take into account the effect of magnetic field on cesium calibration. These additional cesium corrections

are currently being studied.

References

[1] The ATLAS Collaboration, G. Aad et al.: The ATLAS Experiment at the CERN Large Hadron Collider, JINST 3 S08003, 2008.

[2] The ATLAS Collaboration: Tile Calorimeter Technical Design Report, CERN/HCC 96-42, 1996.

[3] Y.A. Kulchitski *et al.,* Electromagetic Cell Level Calibration for ATLAS Tile Calorimeter Modules, ATLAS Note CERN-ATL-TILECAL-PUB-2007-001, CERN, Geneva, 2007.

[4] K.J. Anderson et al., Performance and Calibration of the TileCal Fast Readout Using the Charge Injection System, ATLAS Internal Note ATL-TILECAL-INT-2008-002, CERN, Geneva, 2008.

[5] S. Solodkov: Cesium calibration constants for ATLAS Tile Calorimeter, Tilecal Calibration Workshop, November 2007, http://indico.cern.ch/getFile.py/access?contribId=4&sessionId=2&resId=1&materialId=slides&confId=23070.

[6] R.J Teuscher and T. Davídek, Methods of energy reconstruction in TileCal, http://indico.cern.ch/materialDisplay.py?contribId=s0t6&sessionId=s0&materialId=0&confId=a031558, CERN, Geneva, 2006.

[7] The Tilecal Collaboration, Methods of energy reconstruction in TileCal, http://tilecal.web.cern.ch/tilecal/documents/Testbeam/method_summary/.

[8] S. Agostinelli et al., NIM **A506** (2003) 250–303.

[9] J. Allison et al., IEEE Transactioins on Nuclear Science **53 No.1** (2006) 270–278.

[10] N.A. Shalanda et al., NIM **A508** (2003) 276–286.

[11] J. Abdallah et all (ATLAS Collaboration), The Production and Qualification of Scintillator Tiles for the ATLAS Hadronic Calorimeter, ATLAS Note ATL-TILECAL-PUB-2007-010, CERN, Geneva, 2007.

[12] U. Blumenschein, I. Korolkov and M. Volpi, Calibration Constants for Integrators and Minimum Bias Monitoring, talk given at Tilecal Calibration Workshop, 12th November 2007.

[13] V. Giangiobbe and D. Calvet, Performance of the TileCal super-drawers from a global analysis of the MobiDICK tests, ATL-TILECAL-PUB-2008-007, CERN, Geneva, 2008.

[14] S. Errede et al.: The Effect of Tile Light Collection Reduction along Radius on the ATLAS Tile Calorimeter Uniformity, page 6 and Figure 7, ATLAS Note, ATL-TILE-COM-2008-014, CERN, Geneva, 2008.

[15] H. Hakobyan, M. Simonyan, T. Carli and A. Henriques: Measurement of Pion and Proton Longitudinal Shower Profiles up to 20 Nuclear Interaction Lengths with the ATLAS Tile Calorimeter, ATLAS Note ATL-TILECAL-PUB-2007-008, CERN, Geneva, 2007.

[16] M. Varanda, A. Maio and A. Henriques, Uniformity of the 1996 Barrel Module 0 response to muons and pions: Test beam data and MC simulation, ATLAS Note ATL-TILECAL-99-006, CERN, Geneva, 1996.

[17] E. Starchenko, A. Zenine: Geometrical aspects of Tile Response to Cs source, Tilecal week, October 2001, https://twiki.cern.ch/twiki/bin/view/Atlas/TileCesium, see attachements str.doc and str.ppt, CERN, Geneva.

[18] T. Davídek and A. Henriques: Uniformity with 90 deg muons, July 2008, http://indico.cern.ch/getFile.py/access?contribId=29 &sessionId=2&resId=0&materialId=slides&confId=31921, CERN, Geneva.

[19] Z. Ajaltouni et al., NIM **A388** (1997) 64–78.

[20] L. Přibyl, Muon weights from projective muon runs, talk on Pion Taskforce Meeting, June 18 2008, http://indico.cern.ch/getFile.py/access?contribId=5&resId=1&materialId=slides&confId=36058, CERN, Geneva.

[21] G. Schlager: The Energy Response of the ATLAS Calorimeter System, section 9.2, CERN-THESIS-2006-056, CERN, Geneva.

[22] M. Cascella: Analisi del segnale rilasciato dai muoni di alta energia nel calorimetro adronico dell'esperimento ATLAS, Diploma Thesis, INFN, Sezione di Pisa, Italy, 2006.

[23] T. Davídek and R. Leitner: Parametrization of the Muon Response in the Tile Calorimeter, ATLAS Note ATL-TILECAL-97-114, 1997, CERN, Geneva.

[24] G. Schlager: The Energy Response of the ATLAS Calorimeter System, page 165, Fig. 9.32, CERN-THESIS-2006-056, CERN, Geneva.